JOURNAL OF PETROLOGY | VOLUME 41 | NUMBER 6 | PAGES 789–808 | 2000

Primitive Magma From the Jericho Pipe, N.W.T., Canada: Constraints on Primary Kimberlite Melt Chemistry

S. E. PRICE, J. K. RUSSELL* AND M. G. KOPYLOVA

IGNEOUS PETROLOGY LABORATORY, DEPARTMENT OF EARTH AND OCEAN SCIENCES, UNIVERSITY OF BRITISH COLUMBIA, VANCOUVER, B.C., CANADA, V6T 1Z4

RECEIVED APRIL 23, 1999; REVISED TYPESCRIPT ACCEPTED NOVEMBER 15, 1999

We report the first estimates of primary kimberlite melt composition from the Slave craton, based on samples of aphanitic kimberlite from the Jericho kimberlite pipe, N.W.T., Canada. Three samples derive from the margins of dykes where kimberlite chilled against wall rock (JD51, JD69 and JD82) and are shown to be texturally consistent with crystallization from a melt. Samples JD69 and JD82 have geochemical characteristics of primitive melts: they have high MgO (20–25 wt %), high mg*-numbers (86–88), and high Cr (1300–1900 ppm) and Ni (800–1400 ppm) contents. They also have high contents of CO_2 (10–17 wt %). Relative to bulk macrocrystal kimberlite, they have lower* mg*-numbers and lower MgO but are enriched in incompatible elements (e.g. Zr, Nb and Y), because the bulk kimberlite compositions are strongly controlled by accumulation of mantle olivine and other macrocrysts. The compositions of aphanitic kimberlite from Jericho are similar to melts produced experimentally by partial melting of a carbonate-bearing garnet lherzolite. On the basis of these experimental data, we show that the primary magmas from the Jericho kimberlite could represent 0·7–0·9% melting of a carbonated lherzolitic mantle source at pressures and temperatures found in the uppermost asthenosphere to the Slave craton. The measured CO_2 contents for samples JD69 and JD82 are only slightly lower than the CO_2 contents of the corresponding experimental melts; this suggests that the earliest hypabyssal phase of the Jericho kimberlite retained most of its original volatile content. As such these samples provide a minimum CO_2 content for the primary kimberlite magmas from the Slave craton.*

KEY WORDS: *kimberlite; melt; primitive; primary magma; Slave craton*

INTRODUCTION

The chemical composition and physical character of primary kimberlite magma remains enigmatic because of the difficulty of isolating material that unambiguously represents the melt phase (Foley, 1990; Scott Smith, 1996). There are, for example, no occurrences of quenched 'glassy' kimberlite (Mitchell, 1986). The problem is compounded further by the hybrid nature of most kimberlites, which contain a mixture of mantle and crustal xenoliths, diverse numbers of large (0·5–10 mm) phenocrysts or xenocrysts (e.g. macrocrysts), subordinate amounts of cognate microphenocrysts and groundmass material (Mitchell, 1986; Foley, 1990; Scott Smith, 1996).

In the absence of kimberlitic glasses, aphanitic samples of kimberlite probably represent the next best approximation to the melt phase. Aphanitic samples (e.g. <5 vol. % macrocrysts) of kimberlite are relatively rare, especially in hypabyssal facies kimberlite (Scott Smith, 1996). Examples described in the literature include samples from the Wesselton mine (Shee, 1986), the Mayeng Kimberlite Sill Complex (Apter *et al.*, 1984) and Benfontein (Mitchell, 1997) from South Africa, the Koidu kimberlite complex from West Africa (Taylor *et al.*, 1994), and the Aries kimberlite from Western Australia (Edwards *et al.*, 1992). Of these examples, only the Wesselton and Benfontein examples are Group I kimberlite; all others are Group II (orangeite; Mitchell, 1995).

The focus of our research has been to isolate and sample material within the Jericho kimberlite, Northwest Territories, Canada (Fig. 1), that represents the melt phase. Within this paper we have three goals: (1) we

*Corresponding author. Telephone: 604-822-2703. Fax: 604-822-6088. e-mail: russell@perseus.geology.ubc.ca

demonstrate that, texturally and geochemically, some aphanitic kimberlite samples represent the melt phase at the time of emplacement; (2) we provide a comprehensive chemical characterization of these samples and compare them with compositions of other primitive kimberlite candidates (e.g. Mitchell, 1986, 1995; Shee, 1986; Berg, 1998; Berg & Carlson, 1998); (3) we show that our best estimates of kimberlite melt are similar to compositions of melts produced experimentally by partial melting of carbonated peridotite (e.g. Canil & Scarfe, 1990; Dalton & Presnall, 1998). Our data provide the first constraints on the nature of primary mantle-derived kimberlite melts from beneath the Slave craton.

JERICHO KIMBERLITE

Geology of the Jericho pipe

The Jericho pipe is a diamondiferous kimberlite body situated 400 km NE of Yellowknife near the northern end of Contwoyto Lake (Fig. 1). Previous studies have documented the geology and emplacement history of the pipe (Fig. 2; Cookenboo, 1998), the petrography and geochemistry of the kimberlite (Kopylova *et al.*, 1998*a*), and the petrology and thermal state of the underlying mantle (Kopylova *et al.*, 1998*b*, 1999; Russell & Kopylova, 1999). The Jericho kimberlite intrudes the Archean Contwoyto granitic batholith and, at depth, cuts older Precambrian mafic dykes.

The pipe comprises three distinct phases of kimberlite (Fig. 2). Phase 1 is the earliest and comprises a series of hypabyssal kimberlite intrusions that represent a precursor set of dykes. Phase 1 kimberlite also contains autoliths or fragments of fine-grained kimberlite that derive from the earliest kimberlite intrusion. Phase 2 and Phase 3 represent progressively later pulses of kimberlite. Individual phases are distinguished by colour, texture, degree of serpentinization, mantle xenolith and xenocryst content, magnetic susceptibility and density (Cookenboo, 1998). There are enough trace element similarities between phases to suggest that they derived from the same batch of kimberlite magma (Kopylova *et al.*, 1998*a*).

The Jericho kimberlite incorporates both crustal and mantle xenoliths (Kopylova *et al.*, 1999). Crustal xenoliths include granite and Middle Devonian fossiliferous limestone xenoliths (Cookenboo *et al.*, 1998). Mantle-derived xenoliths mainly comprise low-T and high-T peridotite (60%) of lherzolitic and harzburgitic composition. The remainder of mantle xenoliths include eclogite (25%), pyroxenite (9%) and other rock types. Thermobarometric studies of these xenoliths (Kopylova *et al.*, 1998*b*, 1999) show that these mantle samples derive from depths of 40–220 km; this corresponds to equilibration pressures of 1·5–6·5 GPa. Deformed, high-T peridotite samples that depart from the steady-state conductive geotherm may record a thermal event associated with the production of kimberlite, and these samples record equilibration pressures between 5 and 6·8 GPa (e.g. Kopylova *et al.*, 1998*a*, 1999; Russell & Kopylova, 1999).

Kimberlite samples

The Jericho body is a non-micaceous Group Ia kimberlite (Kopylova *et al.*, 1998*a*) based on the classification scheme of Smith *et al.* (1985). The pipe comprises mainly hypabyssal, macrocrystal, calcite serpentine kimberlite (Kopylova *et al.*, 1998*a*). The term macrocryst refers to the large (>0·5 mm) crystals that commonly dominate most kimberlite (Mitchell, 1986; Scott Smith, 1996). The term is not genetic, in that it applies to both xenocryst and phenocryst material. At Jericho the macrocryst assemblage includes olivine, phlogopite, ilmenite, pyroxene and garnet. Following Scott Smith (1996) we restrict the term microphenocryst to crystals that are <0·5 mm in size and possibly cognate. Aphanitic kimberlite refers to those samples containing <5% macrocrysts.

The results we present below are based on data from four samples of aphanitic kimberlite collected from the margins of the Jericho kimberlite pipe (Cookenboo, 1998). The samples are all associated with the Phase 1 hypabyssal intrusions (Fig. 2), and descriptions of the field relationships are summarized in Table 1. Samples JD51, JD69 and JD82 represent the fine-grained (Fig. 3a–c), chilled material along the margins of thin (<5 m) kimberlite dykes. These aphanitic samples contain virtually no macrocrysts and may represent magma in which macrocrysts were never present (truly aphyric magma). Sample LGS07 (Fig. 3d) has been described by Kopylova *et al.* (1998*a*) and derives from the aphanitic margins of a Phase 1 kimberlite body that has intruded and cooled against earlier Phase 1 macrocrystal kimberlite (Fig. 3e). It inherits its aphanitic character from flow differentiation processes, where the largest macrocrysts have been physically sorted and removed during ascent or emplacement (e.g. Bhattacharji, 1967; Komar, 1972; Mitchell, 1986; Scott Smith, 1996).

Petrography

The basic mineralogy and petrology of the Jericho kimberlite have been described by Kopylova *et al.* (1998*a*). All three phases have a common mineralogy including microphenocrystal olivine and a groundmass assemblage of calcite, serpentine, spinel, apatite, perovskite and ilmenite. We have provided additional petrographic descriptions for the aphanitic kimberlite samples that form the basis for this work (Table 1). The groundmass mineralogy was identified and studied on polished thin sections using conventional transmitted and reflected light

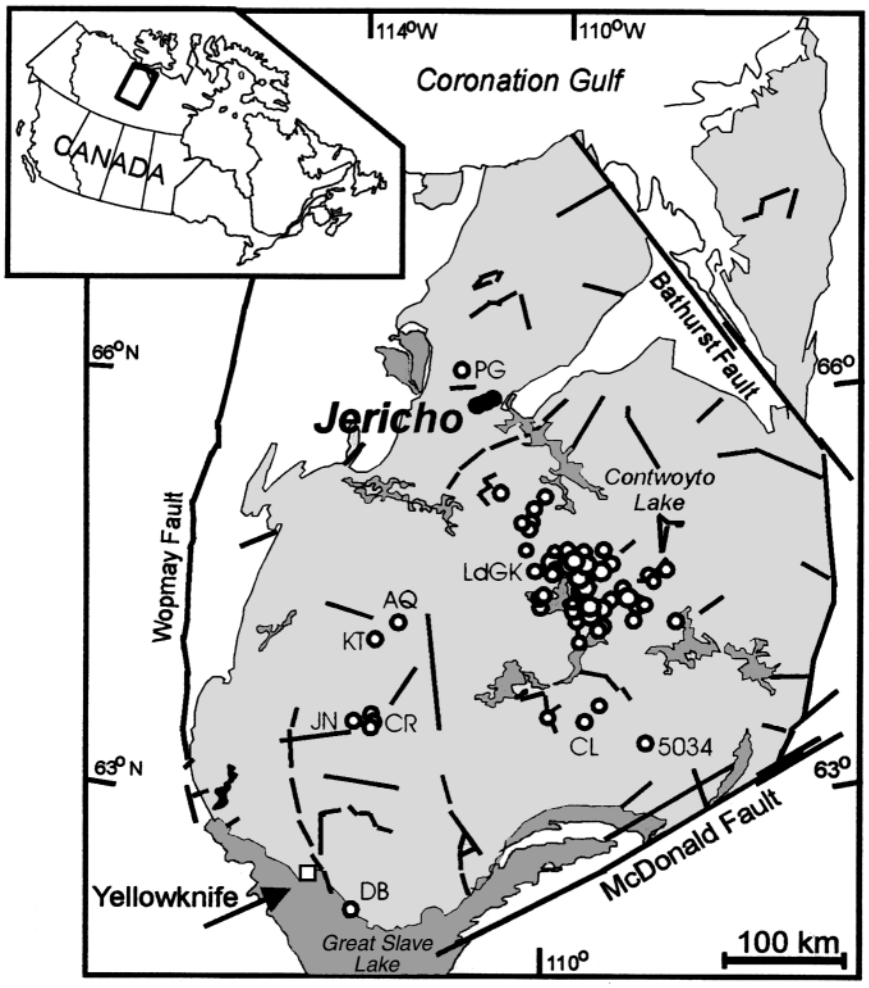

Fig. 1. Distribution of kimberlite pipes (○) in the Slave craton, NW Canada (see inset). Specific pipes shown on map include: ●, Jericho; PG, Peregrine; LdGK, the Lac de Gras kimberlite field; AQ, Aquila; KT, Kent; JN, Jean; CR, Cross cluster; CL, CL-25; 5034, Kennedy Lake; DB, Drybones.

optical microscopy, and scanning electron microscopy (SEM) with a Philips XL30 instrument in conjunction with semi-quantitative chemical analyses of mineral grains by energy-dispersive spectrometry (EDS) using a Princeton Gamma-Tech instrument.

Modal abundances of groundmass minerals (Table 1) were estimated from back-scattered electron SEM images collected at $\sim 100\times$ magnification. Modes were estimated from false colour images produced from original BSE data; conversion to false colour images was optimized so as to maximize discrimination between individual phases (Price, 1998). All image processing was handled by the built-in scanning electron microscope image analysis software. The major phases, including calcite, serpentine, olivine and apatite, were easily identified on the basis of BSE images. However, precise determination of modes for accessory phases (e.g. perovskite, Fe–Ti oxides) was not possible because of low abundances, irregular distributions and similar mean atomic numbers.

Samples of chill margins, represented by JD51, JD69 and JD82, are very fine grained and texturally uniform (Fig. 3a–c). They show no evidence of macroscopic or microscopic mineral alignment or other features indicative of flow differentiation and mainly contain small numbers of altered olivine microphenocrysts (<0·3 mm) set in a groundmass of calcite, serpentine and oxides (Fig. 3a–c). Accessory groundmass phases include perovskite, chromian spinel, ilmenite, Ni–Fe-sulphides, apatite, phlogopite and barite (Fig. 3c). Sample JD51 has the highest content of calcite (39 vol. %) followed by JD69 (30 vol. %), and then JD82 (26 vol. %). JD51 also contains calcite–serpentine segregations, which are typical of hypabyssal facies kimberlite (Mitchell, 1986). In summary, chilled margin samples JD51, JD69 and JD82 share textural and mineralogical

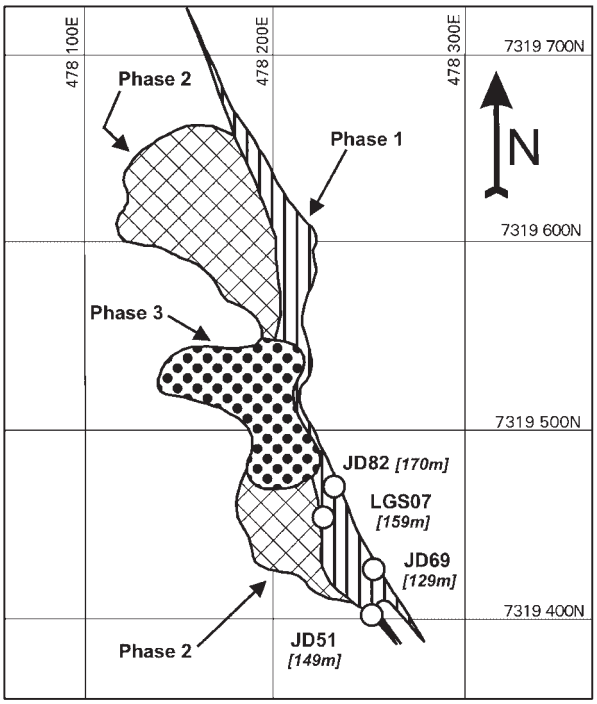

Fig. 2. Plan view (grid interval 100 m) of the Jericho kimberlite pipe at 50 m depth showing distribution of three phases of kimberlite as mapped by Cookenboo (1998) and locations (○) of aphanitic kimberlite samples. Sample depths are recalculated for an average surface elevation of 493 m above sea level.

characteristics consistent with *in situ* crystallization from a relatively crystal-free melt.

Sample LGS07 has been described, in part, by Kopylova *et al.* (1998*a*). It has a hypabyssal texture with fresh (unserpentinized), subhedral to rounded grains of olivine (Fig. 3d) set in a serpentine plus calcite (21 vol. %) groundmass with a high proportion (12 vol. %) of accessory minerals. This sample contains a much higher proportion (~50 vol. %) of larger, subrounded olivine grains (Fig. 3d) than found in the aphanitic samples described above. In fact, although LGS07 is finer grained than macrocrystal Phase 1 kimberlite, there are some parallels. The proportion of olivine grains to groundmass is high and the olivine grains show a variety of size distributions (compare Fig. 3d with Fig. 3e). The sample also shows a weak alignment of macrocrysts that is probably imparted by flowage (e.g. Bhattacharji, 1967; Komar, 1972). On the basis of these observations, LGS07 may represent a 'micro-macrocrystal' facies of kimberlite in which the olivine macrocrysts have been milled during transport and emplacement. Conversely, the olivine may result from the accumulation of cognate crystals and the rounding may be due to partial serpentinization. In either case, although LGS07 is aphanitic, the proportion of the sample that represents melt is small.

GEOCHEMISTRY

Despite the limited amount of aphanitic material available at each locality, we collected three separate samples of JD69, JD82 and LGS07. All samples were treated independently, to provide a measure of sample heterogeneity and analytical reproducibility. Only sufficient material for a single aliquot of JD51 was available.

Sample preparation

All macroscopic xenolithic material was removed after an initial coarse crushing of the samples. The samples were then cleaned with compressed air and passed through a steel-faced jaw crusher to reduce the size to <0·5 cm. At this stage, because our objective was to constrain the composition of the melt phase, we handpicked the sample to remove as many macrocrysts (>0·5 mm) as possible. The maximum macrocryst content found in these samples was ~3%, but handpicking reduced this to <1%. The macrocryst assemblage is dominated by olivine, which moves the bulk composition of kimberlite samples to higher values of MgO, SiO_2 and FeO, and towards lower CaO and CO_2 contents. Some macrocrysts may represent cognate material (e.g. phenocrystic olivine); however, there is no means of accurately distinguishing between xenocrystic and phenocrystic macrocrysts. By extracting all macrocrysts we ensured that only the melt phase was sampled.

Handpicked material included partly serpentinized olivine, dark green books of serpentine (pseudomorphs after olivine), and rare grains of dark pink (peridotitic) and orange (eclogitic) garnets. These samples were then powdered to ~100 mesh using a tungsten carbide ring mill before geochemical analysis.

Analytical procedures

The samples were analysed for major and trace element concentrations, and for oxygen and carbon isotope abundances. Major element, trace element, CO_2, H_2O^+, H_2O^- and loss on ignition (LOI) abundances were determined at the Geochemical Laboratories of McGill University, Montreal, Quebec. Major and trace elements were measured by X-ray fluorescence (XRF) spectrometry using a Philips PW2400 spectrometer. The major elements Si, Ti, Al, Fe, Mn, Mg, Ca, Na, K and P, and the trace elements Ba, Cr, Ni and V were determined on fused beads, whereas pressed powder pellets were analysed for the trace elements Rb, Sr, Nb, Zr, Y, Pb, Ga, Th and U. Total iron (Fe_2O_3) was determined by XRF; ferrous iron was determined volumetrically. H_2O determinations were made by difference and CO_2 concentrations were measured using a

Table 1: Jericho aphanitic kimberlite sample descriptions and groundmass mineralogy

Sample	Size (cm^3)	Sample description and contact relationships	Mineralogy* (vol. %)			
			Olivine	Serpentine	Calcite	Other
JD51	100	Light grey, competent, aphanitic kimberlite with no obvious alteration. Bounded by macrocrystal Phase 1 kimberlite above and bounded below by a thin mafic dyke (sharp contact with no obvious brecciation). Small numbers of microphenocrysts	—	58	39	3
JD69 (-1) (-2) (-3)	560	Light grey, moderately friable, aphanitic kimberlite. Rare microphenocrysts are serpentinized. Bounded by upper contact against macrocrystal Phase 1 kimberlite and a lower brecciated contact against mafic dyke	—	68	30	2
JD82 (-1) (-2) (-3)	560	Light grey, moderately friable, aphanitic kimberlite. Rare microphenocrysts are completely serpentinized. Bounded by macrocrystal Phase 1 kimberlite above and by a mafic dyke below	—	70	26	4
LGS07	200	Dark grey, competent, aphanitic kimberlite. Bounded by macrocrystal Phase 1 kimberlite above (with gradually coarsening contact over ~10 cm) and by macrocrystal Phase 1 kimberlite below (sharp contact). Sample was split into LGS07-1, LGS07-2 and LGS07-3 (Kopylova *et al.*, 1998*a*). Abundant microphenocrysts	15	52	21	12

*Modal abundances were estimated using false colour BSE images, except for sample LGS07 (Price, 1998).

LECO induction furnace and absorption bulb. Rare earth element (REE) concentrations were measured by inductively coupled plasma-mass spectrometry (ICP-MS) on an Elan-5000 instrument at the Department of Geological Sciences, University of Saskatchewan, Saskatoon, following procedures of Jenner *et al.* (1990).

Carbon and oxygen isotopes were measured at the Department of Geological Sciences, Queens University in Kingston, Ontario, using a MAT 252, multi-collector isotope-ratio mass spectrometer. Both isotope ratios were measured for the carbonate fraction and oxygen isotope ratios were determined for the silicate fraction. To prepare the silicate fraction, calcite was removed before analysis, by reaction with 10% HCl. All carbonate in the samples is calcite. The powdered samples were allowed to react for ~2 h, then centrifuged to allow removal of the liquid. This process was repeated with HCl to ensure all calcite was removed, then repeated twice more with deionized H_2O to ensure all residual HCl was removed. No attempt was made to remove the silicate fraction from the calcite fraction.

Major element chemistry

Major element compositions for all samples and average compositions of bulk macrocrystic kimberlite from the Jericho pipe (Kopylova *et al.*, 1998*a*) are presented in Table 2. The replicate samples of JD69 and JD82 generally show small (<5%) variations in major element composition that derive from (1) variable distributions of microphenocrysts, (2) variation induced during sample preparation (e.g. efficiency of handpicking macrocrysts), and (3) variance attributable to analytical uncertainties.

Calculated contamination indices ($CI = SiO_2 + Al_2O_3 + Na_2O)/(MgO + 2K_2O$) for all samples are <1·5 (Table 1; Clement, 1982), consistent with a lack of contamination by crustal rocks. Magnesium numbers [*mg*-number = $100Mg/(Mg + Fe_T)$] for the aphanitic kimberlite samples vary between 82 and 88. The *mg*-numbers for the corresponding bulk kimberlite samples (Table 2) are higher on average (89–90) because of the large content of macrocrystal olivine.

The aphanitic samples show strong linear correlations between SiO_2, CaO and CO_2 and MgO (Fig. 4a, d and e) reflecting the mineralogical controls of olivine, serpentine and calcite. Covariations of SiO_2 and MgO (Fig. 4a) can be explained by controls imposed by serpentine (JD51, JD69, JD82) or by olivine (LGS07). The samples that parallel the olivine-control line, including autoliths of Phase 1 and bulk samples of macrocrystal Phases 1 and 3 kimberlite, contain unaltered olivine microphenocrysts, whereas the samples JD51, JD69 and

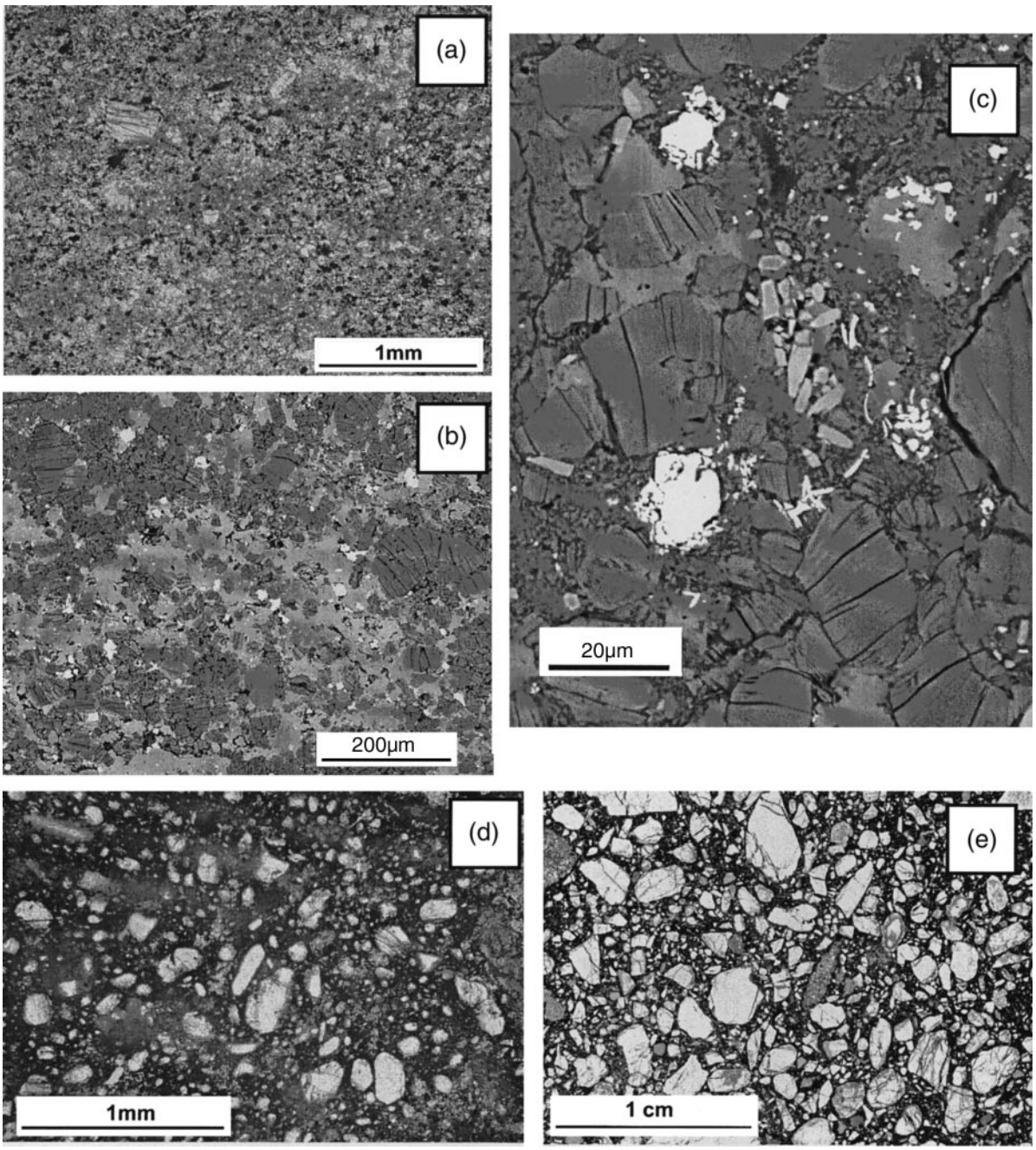

Fig. 3. Petrographic features of kimberlite samples from the Jericho pipe. (a) Photomicrograph (plane-polarized light) of JD51 showing fine-grained, homogeneous, hypabyssal texture. Sparse olivine microphenocrysts are altered. (b) BSE image of JD69 showing fine-grained, homogeneous nature of groundmass composed of serpentine (dark grey), calcite (light grey) and oxides (white). (c) BSE image of groundmass in JD82 comprising serpentine (dark grey) and minor calcite (light grey). Bright grains are chromian spinels and Fe–Ni-sulphides; light-coloured grey stubby grains are apatite. (d) Photomicrograph of sample LGS07 (plane-polarized light). Sample is aphanitic but in thin section is characterized by abundant subhedral to rounded olivine microphenocrysts. (e) Photomicrograph (plane-polarized light) showing character of Phase 1 macrocrystal kimberlite.

JD82, and Phase 2 macrocrystal kimberlite are more serpentinized.

One of the most striking features of these data is the relatively high CO_2 contents of the aphanitic kimberlite samples (Fig. 4e and f). Values for aphanitic kimberlite range from 5 wt % (LGS07) to 18 wt % (JD51), which are substantially higher CO_2 contents than found in samples of macrocrystal kimberlite (Table 2). The CO_2

*Table 2: Major (wt %) and trace element (ppm) compositions of aphanitic kimberlite from Jericho and average (*n*) compositions of autoliths and bulk macrocrystic kimberlite from Kopylova* et al. *(1998a)*

Sample:	JD51	JD69			JD82			LGS07			Autoliths	Phase 1	Phase 2	Phase 3	1 SD*
		69-1	69-2	69-3	82-1	82-2	82-3	07-1	07-2	07-3	$n = 10$	$n = 18$	$n = 10$	$n = 9$	
SiO_2	20·77	24·15	27·00	29·06	28·83	28·13	30·31	34·04	32·90	31·86	30·51	33·04	35·25	33·57	0·197
TiO_2	0·89	0·51	0·51	0·49	0·57	0·71	0·77	0·82	1·05	1·19	1·03	0·99	0·79	0·77	0·005
Al_2O_3	1·82	1·14	1·33	1·38	1·39	1·61	1·75	2·10	2·06	2·25	2·02	1·78	2·76	1·88	0·056
Fe_2O_3	6·47	2·23	2·15	2·13	5·27	2·69	2·95	2·16	2·57	2·82	2·93	2·50	2·68	2·66	0·063
FeO	0·57	3·58	3·50	3·79	1·51	4·17	4·64	5·36	5·17	5·15	4·89	5·51	4·38	4·72	—
MnO	0·19	0·16	0·14	0·13	0·16	0·16	0·15	0·17	0·19	0·20	0·17	0·16	0·13	0·14	0·004
MgO	16·65	19·71	22·39	23·69	23·25	23·09	25·14	35·28	34·41	33·98	32·91	36·12	30·62	34·78	0·217
CaO	25·45	22·25	19·37	16·69	16·86	16·66	13·32	7·12	7·49	8·73	9·46	6·79	6·56	6·64	0·109
Na_2O	0·10	0·14	0·15	0·13	0·12	0·19	0·24	0·15	0·20	0·18	0·12	0·12	0·16	0·12	0·012
K_2O	0·17	0·33	0·43	0·45	0·43	0·46	0·42	0·41	0·26	0·26	0·14	0·16	0·62	0·22	0·012
P_2O_5	0·85	0·67	0·61	0·56	0·71	0·78	0·75	0·68	0·84	0·96	0·48	0·43	0·30	0·24	0·005
CO_2	18·82	16·91	14·01	12·97	12·39	12·06	9·80	4·84	4·91	5·76	6·96	4·75	4·40	5·03	0·01
H_2O^+	5·30	6·40	7·10	6·40	6·00	6·70	7·50	5·24	5·80	5·05	6·19	5·31	7·65	6·89	0·04
H_2O^-	1·02	0·71	0·76	0·76	1·15	1·04	1·05	0·67	0·81	0·56	1·11	0·88	2·05	1·01	
Total	99·07	98·89	99·45	98·63	98·64	98·45	98·79	99·04	98·66	98·95	98·92	98·54	98·35	98·67	
LOI	25·45	24·04	21·98	20·40	20·40	20·11	18·54	10·35	11·37	11·21	14·12	10·91	14·40	12·85	
CI	1·34	1·25	1·22	1·24	1·26	1·25	1·24	1·01	1·01	0·99	0·98	0·96	1·20	1·01	
ILM	0·43	0·3	0·26	0·25	0·28	0·3	0·31	0·23	0·24	0·26	0·26	0·24	0·24	0·22	
Si/Mg	0·97	0·95	0·93	0·95	0·96	0·94	0·93	0·75	0·74	0·73	0·72	0·71	0·89	0·75	
mg-no.	82·3	86·3	88·0	88·1	86·9	86·2	86·0	89·6	89·1	88·7	88·6	89·2	88·9	89·7	
Cr†	2013	1301	1312	1570	1513	1803	1891	2121	2463	2874	1916	1916	1711	1847	18
Ba	666	2889	4026	7274	3351	2820	3318	2160	2100	2370	1188	1637	1173	1054	28
Rb	13·4	23·8	30·0	30·7	26·8	29·3	27·6	66	56	54	20	29	66	34	0·2
Sr	472·0	948·9	692·8	571·7	498·5	423·4	297·2	840	670	958	373	577	413	326	2·7
Nb	263·0	168·7	165·4	142·6	182·0	207·5	231·8	196	246	274	110	143	105	96	1·3
Zr	125·1	71·6	71·3	67·8	73·0	93·8	108·8	96	120	135	49	66	61	47	0·6
Y	12·8	9·6	10·3	11·1	10·2	10·9	11·3	12	12	12	6	7	8	6	0·07
Pb	23·5	13·1	15·7	14·3	15·9	13·2	16·2	10	12	10	4	6	6	6	0·09
Ni	598	789	1099	1151	1291	1367	1396	1350	1200	1100	936	1383	1315	1478	14
V	107	87	87	95	90	85	87	—	—	—	—	—	—	—	0·9
Ga	5·0	1·9	1·8	b.d.	2·8	3·2	3·0	—	—	—	—	—	—	—	0·02
Th	35·1	18·5	16·6	15·0	19·8	25·7	28·8	—	—	—	—	—	—	—	0·2
U	5·0	1·0	b.d.	b.d.	b.d.	b.d.	b.d.	—	—	—	—	—	—	—	0·3

LOI, loss on ignition; CI (Contamination Index) = $(SiO_2 + Al_2O_3 + Na_2O)/(MgO + 2K_2O)$, after Clement (1982); ILM (Ilmenite Index) = $[FeO(t) + TiO_2]/(MgO + 2K_2O)$, after Taylor *et al.* (1994); *mg*-number = $100Mg/(Mg + Fe_T)$; b.d., below detection (detection limit for U and Th is 1·0 ppm); —, elements not determined.
*Analytical uncertainty (1 SD) is based on replicate analyses (e.g. Russell & Snyder, 1997).
†Cr (ppm) for LGS07 samples was recalculated from Cr_2O_3 (wt %).

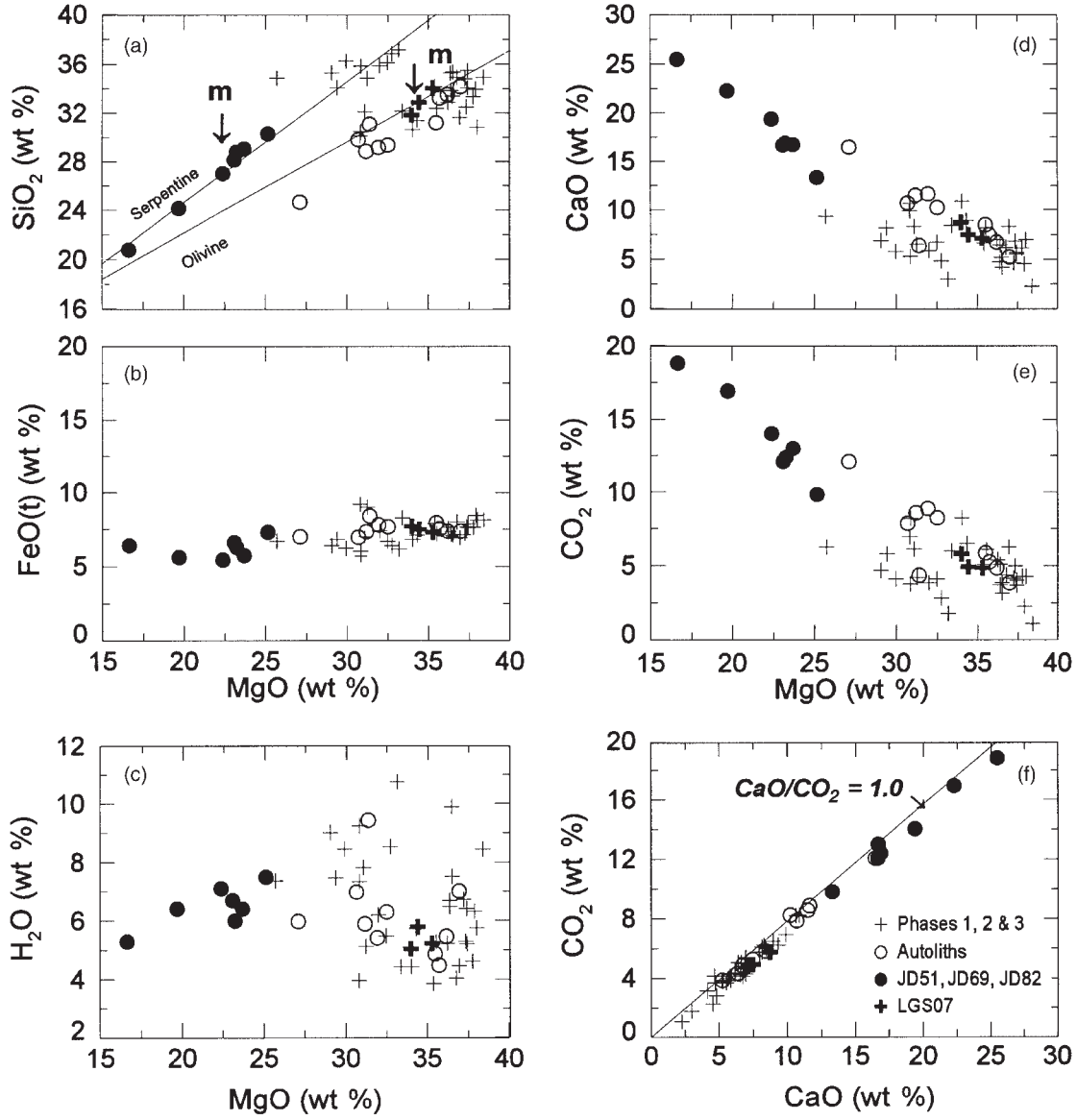

Fig. 4. Chemical compositions of aphanitic samples are compared with compositions of bulk kimberlite from Jericho. Compositions are plotted as: (a) SiO_2 vs MgO; (b) FeO(t) vs MgO; (c) H_2O vs MgO; (d) CaO vs MgO; (e) CO_2 vs MgO; (f) CO_2 vs CaO. Chemical data for autoliths, Phases 1–3 and sample LGS07 derive from Kopylova *et al.* (1998*a*). Mineralogical control lines for end-member serpentine (Si/Mg = 0·67) and forsterite (Si/Mg = 0·5) are plotted in (a) and are forced through points JD69-2 and LGS07-2, respectively (denoted as 'm'). Line for calcite control is plotted in (f) (see text).

content correlates directly with calcite content; Fig. 4f shows that variations in CaO and CO_2 contents mimic exactly the stoichiometry of calcite. FeO and H_2O contents of these samples vary only slightly and show substantially less variation than recorded by macrocrystal kimberlite samples.

An important aspect of the data shown in Fig. 4 is that samples JD51, JD69 and JD82 plot along trends that extrapolate to macrocrystal kimberlite values. Relative to bulk samples of macrocrystal kimberlite, the aphanitic samples have lower MgO and SiO_2 and higher CaO and CO_2. Fine-grained autoliths of Phase 1 kimberlite plot between the two groups. LGS07, on the other hand, plots with the macrocrystal kimberlite. We interpret this pattern to mean that JD51, JD69 and JD82 are estimates of liquid composition whereas the bulk kimberlite compositions are mixtures of the melt phase (possibly the same) plus macrocrystal mineral assemblages. The composition of LGS07 is not representative of a liquid, but it reflects the accumulation of macrocrysts (Figs 3d and 4).

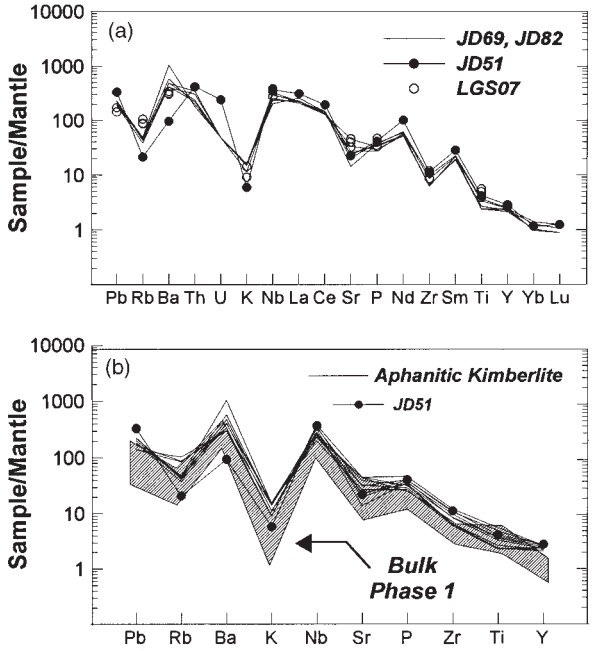

Fig. 5. Primitive mantle normalized multi-element diagrams. (a) Compositions of all aphanitic samples of kimberlite including replicate analyses of JD69 and JD82 (continuous lines), LGS07 (○) and a single analysis of JD51 (●). (b) Same data as in (a) shown as continuous lines vs JD51 and the composition of Phase 1 kimberlite from Jericho (shaded pattern). Normalization values are from McDonough *et al.* (1992), except for P (Sun, 1980) and Yb and Lu (Taylor & McLennan, 1985).

Trace element chemistry

Incompatible and compatible elements

The trends of the trace element abundances (Table 2) plotted normalized to primitive mantle (Fig. 5a and b) show little variation between samples of aphanitic kimberlite. In general, these samples show strong relative enrichment in large ion lithophile elements (LILE) (with the exception of K) and high field strength elements (HFSE), coupled with high light REE (LREE) contents (Fig. 6). Samples are relatively depleted in Rb, K, Sr and Zr. All aphanitic samples have high relative Pb values. Samples JD69, JD82 and LGS07 have similar trace element distributions, but sample JD51 is anomalous in that it is relatively enriched in U and Th and shows slightly higher Nb, La, Ce, Nd and Sm. The enrichment in U and Th may indicate minor crustal contamination, because the host Contwoyto batholith is U and Th rich (Davis, 1991; Legault & Charbonneau, 1993). The aphanitic kimberlite samples are compared with the trace element compositions of Phase 1 bulk kimberlite in Fig. 5b. In terms of distributions of HFSE, the two groups are very similar; however, the aphanitic kimberlite samples show the greatest relative enrichment in trace elements.

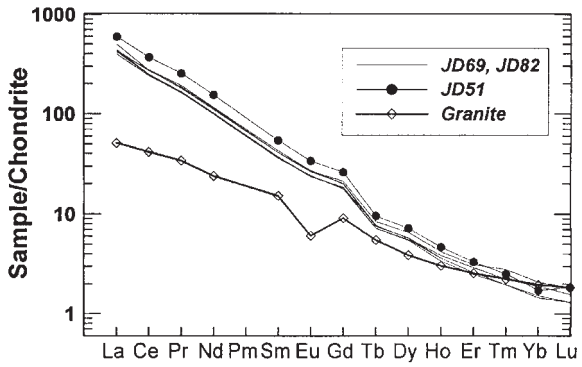

Fig. 6. Chondrite-normalized REE diagram for all aphanitic samples of kimberlite using chondrite values from Taylor & McLennan (1985). Also shown is REE composition of granite from the Contwoyto batholith (Davis, 1991). Analytical uncertainties (Table 3) are equal to or smaller than symbol size.

Rare earth elements

The REE abundances (Table 3) for aphanitic kimberlite are plotted normalized to chondrite (Fig. 6) and show similar ranges in concentration and describe similar patterns. Aphanitic kimberlite samples have extreme LREE enrichment (400–900 times chondrite abundances for La) and show the highly fractionated chondrite-normalized patterns (Table 3; Fig. 6) that are typical of kimberlites world-wide (Mitchell, 1986). The heavy REE (HREE) show fractionation [$(Tb/Lu)_N$ = 4·6–5·9] but substantially less than shown by the LREE [$(La/Sm)_N$ = 9·9–12·1] (Table 3). REE abundances were not determined for sample LGS07 nor for the bulk Jericho samples of Kopylova *et al.* (1998*a*).

Intra-sample variation is slight (Table 3; Fig. 6), with JD51 being somewhat enriched relative to JD69 and JD82. Most samples have $(La/Yb)_N$ values between 230 and 300, except JD51, which is significantly higher (344). JD51 shows anomalous $(La/Yb)_N$ because it has the highest La value and the lowest value of Yb. Mitchell (1986) suggested that contaminated kimberlites are generally enriched in HREE. However, the Contwoyto granite, which is the major country rock in the area, has substantially lower concentrations of LREE and has lower to equal amounts of HREE compared with the Jericho aphanitic kimberlite (Fig. 6). This could help mask the trace element effects of contamination (e.g. JD51).

Other trace elements

Cr and Ni concentrations are high in the aphanitic samples (Table 2) with Cr concentrations ranging between 1300 and 2874 ppm (highest in LGS07) and Ni concentrations ranging between 600 and 1400 ppm. These high values are indicative of primitive mantle

Table 3: Measured REE abundances (ppm) for aphanitic kimberlite from Jericho

Sample:	JD51	JD69			JD82			1 SD*
		69-1	69-2	69-3	82-1	82-2	82-3	
La	218·73	154·51	161·45	182·50	146·20	159·12	155·79	1·659
Ce	353·76	236·85	238·11	263·19	230·60	258·73	264·62	3·681
Pr	34·81	22·81	22·40	24·69	22·20	25·30	26·19	0·584
Nd	109·48	72·26	70·51	78·32	70·60	80·79	82·36	1·376
Sm	12·59	8·58	8·56	9·53	8·32	9·52	9·91	0·057
Eu	2·95	2·08	2·05	2·34	2·11	2·31	2·38	0·046
Gd	8·03	5·61	5·69	6·53	5·46	6·19	6·14	0·128
Tb	0·56	0·42	0·45	0·49	0·42	0·45	0·44	0·0058
Dy	2·76	2·13	2·19	2·51	2·09	2·20	2·23	0·0058
Ho	0·40	0·31	0·33	0·36	0·29	0·31	0·31	0·0058
Er	0·83	0·65	0·73	0·78	0·62	0·65	0·65	0·032
Tm	0·09	0·07	0·08	0·10	0·07	0·07	0·07	0·000
Yb	0·43	0·38	0·47	0·52	0·38	0·36	0·36	0·026
Lu	0·07	0·05	0·06	0·07	0·05	0·05	0·05	0·006
$(La/Yb)_N$	343·7	274·8	232·1	237·2	260·0	298·7	292·4	
$(La/Sm)_N$	10·9	11·3	11·9	12·1	11·1	10·5	9·9	
$(Tb/Lu)_N$	5·3	5·5	4·9	4·6	5·5	5·9	5·8	

*Standard deviation based on three replicate analyses of JD51.

melts and overlap values for samples of autoliths and macrocrystal kimberlite (Phases 1–3) from Jericho (Table 2; Kopylova *et al.*, 1998*a*).

Zr and Nb are elements that are relatively unaffected by small amounts of crustal contamination and immune to the effects of hydrothermal alteration (e.g. Taylor *et al.*, 1994). Kopylova *et al.* (1998*a*) showed a progressive trend in composition from an early Zr- and Nb-enriched phase of the Jericho kimberlite (e.g. Phase 1) to later relatively depleted phases (Fig. 7a; Phases 2 and 3). The aphanitic samples have the highest Nb and Zr values, followed by autoliths and macrocrystal kimberlite from Phase 1, and by Phase 2 and 3 kimberlite (Fig. 7a). The data are described well by a straight line of slope 0·48 and a zero intercept; the latter attribute is consistent with both Zr and Nb behaving incompatibly. We interpret this as indicating that the original melt had a Zr/Nb ratio of 0·48 and that the bulk kimberlite samples have lower Zr and Nb contents because of dilution of the melt phase with accumulated macrocrystic material. The most macrocryst-rich samples have the lowest Zr and Nb contents. Zr and Nb partition into ilmenite, and ilmenite occurs both as macrocrysts and as a groundmass constituent in the Jericho kimberlite; however, the effects of ilmenite sorting are minor compared with the dilution effects of the other macrocrysts (Fig. 7a).

As used by Kopylova *et al.* (1998*a*), P_2O_5 and K_2O can discriminate chemically between individual phases of the Jericho kimberlite (Fig. 7b). The compositions of aphanitic kimberlite samples show a wide range in K_2O content that overlaps other phases of the Jericho kimberlite. However, the aphanitic samples show the highest P_2O_5 contents. Autoliths from Phase 1 kimberlite have similar concentrations of P_2O_5, whereas all other phases have lower values. The lower P_2O_5 contents found in bulk macrocrystal kimberlite (e.g. Phases 2 and 3) may also indicate dilution by accumulation of low-P_2O_5 macrocrystic material.

Stable isotopes

Samples JD51, JD69(-2) and JD82(-2) were analysed for oxygen and carbon isotopes (Table 4). Standard 'δ' notation in parts per thousand (‰) is used relative to the Pee Dee Belemnite (PDB) standard for carbon isotope ratios, and the Standard Mean Ocean Water (SMOW) standard for oxygen isotope ratios (e.g. Hoefs, 1997).

The yields for samples JD51, JD69 and JD82 are >90% of the calculated theoretical yields (Table 4; Fig.

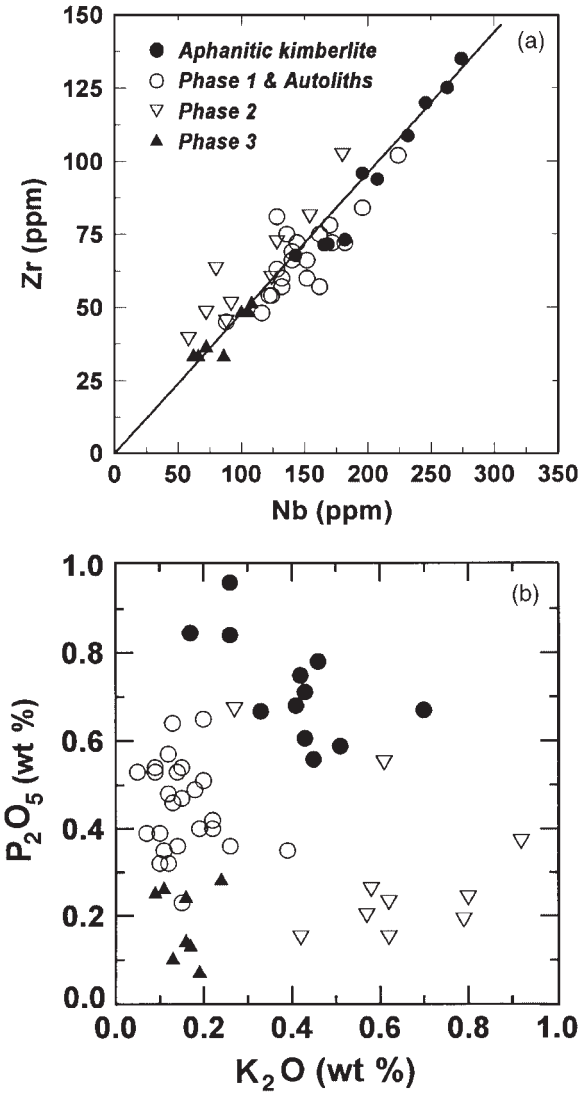

Fig. 7. Trace and minor element compositions of aphanitic kimberlite samples compared with bulk kimberlite from the Jericho pipe, including compositions of Phase 1 (and autoliths of Phase 1), Phase 2 and Phase 3 kimberlite (Kopylova *et al.*, 1998*a*). (a) Compositions plotted as Zr vs Nb describe a linear trend with a mean slope (Zr/Nb) of 0·48 (continuous line). (b) Aphanitic samples are enriched in P_2O_5, relative to individual phases of the Jericho kimberlite.

8a). The measured variation between samples is roughly the same magnitude as that attributable to analytical variance (Table 4). The range of values of $\delta^{18}O_{SMOW}$ (6·2–8·2‰) is narrow, lies within the range established for mica and serpentine found in kimberlite groundmass, and is consistent with derivation from mantle sources (Fig. 8a; Sheppard & Dawson, 1975; Hoefs, 1997). Samples JD51, JD69 and JD82 have been altered as evidenced by the serpentinization of groundmass olivine, but the oxygen isotopic data preclude the involvement of meteoric fluids in this process.

Table 4: Carbon and oxygen isotopic compositions of aphanitic kimberlite

	JD51	JD69 (-2)	JD82 (-2)	SD*
Calcite fraction				
$\delta^{13}C_{PDB}$	−5·2	−4·5	−4·8	0·1
$\delta^{18}O_{SMOW}$	16·6	16·1	16·3	0·2
% Yield†	88	91	96	
Silicate fraction				
$\delta^{18}O_{SMOW}$	8·2	6·2	6·4	1·4
% Yield†	91	95	96	

*SD based on replicate analyses of calcite (n = 4) and silicate (n = 2) fractions of JD69(-2).
†Actual yield/theoretical yield (× 100).

Carbon isotope ratios ($\delta^{13}C$) for the carbonate fraction of samples JD51, JD69 and JD82 vary from –4·5 to –5·2 and have a mean value of $\delta^{13}C_{PDB} = -4{\cdot}6 \pm 0{\cdot}4$‰ (Table 4; Fig. 8b). The extracted yields for these samples are also high (Table 4). The $\delta^{13}C$ values are consistent with estimated values for mantle rocks and are very close to the mean values estimated for the world-wide distribution of kimberlite (Deines & Gold, 1973; Kobelski *et al.*, 1979; Kirkley *et al.*, 1989; Hoefs, 1997). These data strongly support a primary, rather than secondary, origin for the groundmass carbonate in these samples of aphanitic kimberlite.

The oxygen isotope ratios ($\delta^{18}O_{SMOW}$) for the carbonate fractions of Jericho kimberlite have a mean value of 16·2 ± 0·4‰ (Fig. 8b). These numbers are somewhat higher than expected for carbonate in exchange equilibrium with olivine with a $\delta^{18}O_{SMOW}$ of 6–8‰ (Fig. 8a). However, they are consistent with the field established for other kimberlite occurrences (e.g. Deines & Gold, 1973; Kobleski *et al.*, 1979; Hoefs, 1997). They have slightly higher $\delta^{18}O$ values than recorded by samples of Wesselton kimberlite (Kobelski *et al.*, 1979; Kirkley *et al.*, 1989). Furthermore, the $\delta^{18}O$ values for the carbonate fraction are significantly lower than values for marine sediments (e.g. >20; Hoefs, 1997) and are inconsistent with a meteoric fluid source (e.g. <0; Hoefs, 1997).

PRIMARY KIMBERLITE MAGMA

Nature of primitive melts at Jericho

We argue that JD69, JD82 and JD51 represent samples of melt from the Jericho kimberlite. All three samples are from the aphanitic margins of thin (<5 m) hypabyssal

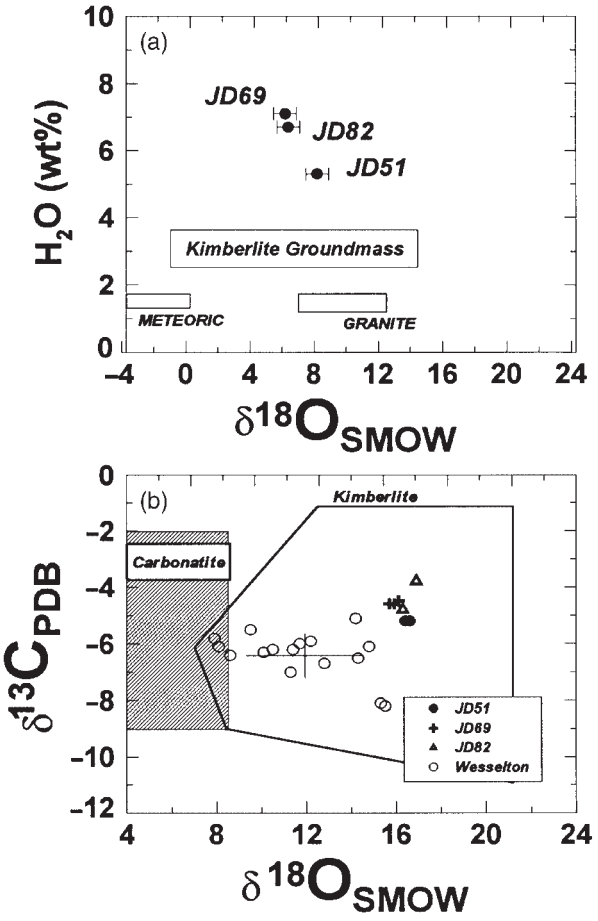

Fig. 8. Carbon and oxygen isotopic compositions of aphanitic kimberlite. (a) $\delta^{18}O$ values for silicate fractions vs H_2O (wt %). Error bars are 1 SD based on duplicate analyses. All samples plot within range of values established for kimberlite based on groundmass serpentine and mica (Sheppard & Dawson, 1975). (b) Values of $\delta^{13}C$ and $\delta^{18}O$ for carbonate from Jericho kimberlite compared with fields established for other kimberlite occurrences, for primary carbonatite (from Deines & Gold, 1973) and Wesselton kimberlite (Kobelski *et al.*, 1979; Kirkley *et al.*, 1989). Fine crossed line shows mean kimberlite composition and 1 SD.

kimberlite dykes. Texturally and mineralogically they indicate crystallization of a melt: they contain few, if any, macrocrysts, and have fine-grained, homogeneous groundmasses. Replicate samples and analyses of two chill margin localities (JD69 and JD82) show little chemical variation (Table 2), as we would expect of samples crystallizing from a uniform melt.

Geochemically, samples JD69 and JD82 represent superior estimates of primitive magma compositions to the Jericho kimberlite. They contain 20–25 wt % MgO and have high *mg*-numbers (86–88). However, they have lower *mg*-numbers than the bulk macrocrystic samples (*mg*-numbers 89–90), which are affected by accumulation of mantle olivine and other macrocrysts. The chill margin samples have high Cr (1300–1900 ppm) and Ni (800–1400 ppm) contents and are enriched in incompatible elements (e.g. Zr, Nb and Y) relative to bulk macrocrystal kimberlite. Sample JD51 has many of the same attributes but contains substantially lower MgO, has an *mg*-number of 82, has a higher contamination index (Table 2) and has anomalous trace element signature relative to the other chill margin samples. Olivine fractionation or minor crustal contamination could be responsible for some of these characteristics.

We have used the Fe–Mg exchange for olivine–carbonate melt given by Dalton & Wood (1993) to calculate the olivine saturation compositions for these liquids (JD69 and JD82). Using their range of K_d values (0·5–0·66) for partitioning of Fe and Mg between olivine and melt, the predicted range of equilibrium olivine compositions is Fo_{92-94} and Fo_{90-92}, respectively (Table 5). These compositions are similar to the most magnesian olivine compositions found in mantle xenoliths from Jericho (Kopylova *et al.*, 1998*a*, 1999) and match the range of compositions for macrocrystal olivine from kimberlite (Scott Smith, 1996). Our melt compositions lie outside the compositional bounds of the Roeder & Emslie (1970) model; however, we have used their model for comparative purposes. The corresponding calculations predict saturation with a substantially more forsteritic olivine (Fo_{95-96}; Table 5).

The aphanitic kimberlite samples also show high, but variable, volatile contents. These samples contain between 12 and 19 wt % CO_2 and between 5·3 and 7·5 wt % H_2O. High CO_2 is manifest as abundant primary calcite in the groundmass (Fig. 3b and c). Aphanitic samples have substantially higher CO_2 contents than macrocrystal kimberlite (Table 2), again, because the latter samples show the effects of dilution of the melt by accumulation of non-volatile bearing macrocrysts. However, the high volatile content of the aphanitic samples strongly suggests that these magmas did not have time to degas completely during transport or between the time of emplacement and crystallization. As such, these analyses provide minimum estimates on the volatile contents of the Jericho kimberlite magmas.

Comparison with other primitive kimberlite

In Table 5, compositions of primitive kimberlite melts from the literature (Wesselton, South Africa; Leslie, N.W.T., Canada; Dutoitspan, South Africa) are compared with the Jericho aphanitic kimberlites and with the average compositions of Group 1A (off-craton; Smith *et al.*, 1985), Group 1B (on-craton; Smith *et al.*, 1985), Kimberley (Clement, 1982) and Siberian kimberlites (Ilupin & Lutz, 1971).

Table 5: Compositions of primitive kimberlites from Jericho, other world-wide occurrences and average compositions of Group I kimberlites; also shown are estimates of F *for Jericho melts and Wesselton kimberlite (see text) and apparent olivine saturation conditions*

	Jericho kimberlite				Other primitive kimberlite			Average Group I kimberlite			
Source:	JD51	JD69*	JD82*	LGS07*	W	L	D	IA	SA	IB	SB
SiO_2	20·77	27·00	28·13	32·90	25·60	31·67	31·73	32·1	30·0	25·7	27·6
TiO_2	0·89	0·51	0·71	1·05	3·35	0·66	1·55	2·0	1·8	3·0	1·6
Al_2O_3	1·82	1·33	1·61	2·06	3·31	1·23	1·94	2·6	2·6	3·1	3·2
Fe_2O_3	6·47	2·15	2·69	2·57	—	9·24	8·76	9·2	9·4	12·7	8·4
FeO	0·57	3·50	4·17	5·17	10·30	—	—	—	—	—	—
MnO	0·19	0·14	0·16	0·19	0·21	0·17	0·16	0·2	0·2	0·2	0·1
MgO	16·65	22·39	23·09	34·41	27·20	40·93	36·17	28·5	29·4	23·8	24·3
CaO	25·45	19·37	16·66	7·49	15·30	8·09	7·98	8·2	10·9	14·1	14·1
Na_2O	0·10	0·15	0·19	0·20	0·28	0·00	0·37	0·2	0·3	0·2	0·2
K_2O	0·17	0·43	0·46	0·26	0·70	0·397	0·74	1·1	1·2	0·6	0·8
P_2O_5	0·85	0·61	0·78	0·84	1·83	0·258	0·80	1·1	1·6	1·1	0·5
CO_2	18·82	14·01	12·06	4·91	4·77			4·3	5·4	8·6	10·8
H_2O^+	5·30	7·10	6·70	5·80	6·20	5·59†	9·85†	8·6	7·3	7·2	7·9
Total	99·07	99·44	98·45	98·66	99·05	99·45	101·24				
Cr	2013	1312	1803	2463	2410			1400	1398	1000	
Ni	598	1099	1367	1200	810			1360	1018	800	
Rb	13	30	29	56	20			50	66	30	
Sr	472	693	423	670	1180			825	1145	1020	
Y	12·8	10·3	10·9	12	10			13	17	30	
Zr	125	71	94	120	580			200	308	385	
Nb	263	165	208	246	250			165	168	210	
Ba	666	4026	2820	2100	1000			1000	915	850	
X_{Fo}‡	90·1–87·6	93·5–91·8	92·5–90·4	94·1–92·5	90·2–87·7	94·5–93·0	94·1–92·5				
X_{Fo}§	94·1	96·2	95·5	96·6	94·2	96·8	96·6				
F (%)	0·466	0·704	0·899	1·066	0·893						
r.m.s.¶	3·02	1·64	1·02	3·86	1·87						

Sources include: W, Wesselton kimberlite, South Africa (Shee, 1986); L, Leslie kimberlite, Canada (Berg & Carlson, 1998); D, Dutoitspan kimberlite, South Africa (Berg, 1998); IA, average of 10 off-craton Group 1A South African kimberlites (Smith *et al.*, 1985); SA, average of 30 kimberlite pipe and dykes from the Kimberley area (Clement, 1982); IB, average of seven on-craton Group 1B South African kimberlites (Smith *et al.*, 1985); SB, average of 623 analyses from Siberia (Ilupin & Lutz, 1971).
*Median samples of three.
†LOI was reported in lieu of CO_2 and H_2O.
‡K_D from Dalton & Wood (1993).
§K_D from Roeder & Emslie (1970).
¶r.m.s. is root mean square of residuals to model solution.

Edgar *et al.* (1988) and Edgar & Charbonneau (1993) argued that the Wesselton aphanitic kimberlite (Table 5) represents unfractionated kimberlite because it contains few olivine macrocrysts, it has low abundances of xenoliths and xenocrysts, and its chemical composition features high MgO content (27%), a high *mg*-number (83–84), low SiO_2 (25·6 wt %), high Ni (810 ppm) and high Cr (2410 ppm) contents. Its composition has been adopted by many others as an example of unfractionated kimberlite magma (Arima *et al.*, 1993; Arima & Inoue, 1995; Mitchell, 1995). Mineral saturation calculations would predict olivine compositions $Fo_{88–90}$ using Dalton & Wood (1993) and Fo_{94} using the Roeder & Emslie (1970) formulation.

In comparison, the aphanitic chill margin samples JD69 and JD82 from Jericho have slightly higher *mg*-numbers, similar SiO_2, higher Ni and slightly lower Cr (Table 2). Wesselton aphanitic kimberlite has 6·2 wt % H_2O, which agrees well with values for Jericho samples (6–7·5 wt %). However, Jericho samples have substantially higher CO_2 contents (10–17 wt %) than found in Wesselton kimberlite (5 wt %). In this regard, the Jericho samples appear to retain more of their original CO_2 content (Foley, 1990; Brey *et al.*, 1991; Dreibus *et al.*, 1995). It is, perhaps, unlikely that the H_2O and CO_2 contents of Jericho samples are primary, but they do establish a minimum CO_2 and H_2O content for the primary magma (e.g. Foley, 1990). In both JD69 and JD82, olivine has been serpentinized; however, the stable isotopic data for these samples (Fig. 8) rule out a meteoric source.

More recently, Berg (1998) has suggested that the hypabyssal Dutoitspan kimberlite, South Africa, and the hypabyssal Leslie kimberlite from N.W.T., Canada (Berg & Carlson, 1998), represent primitive kimberlite magmas (Table 5). That study, however, was based on samples of macrocrystal kimberlite and much of the olivine within the kimberlite is demonstrably xenolithic and derived from peridotite (Berg, 1998).

Experimental constraints on primary melt composition

From experimental studies, kimberlite magma is thought to originate from low degrees of partial melting of carbonate-bearing garnet lherzolite (e.g. Eggler, 1975, 1978; Wyllie, 1977, 1980; Canil & Scarfe, 1990; Edgar & Charbonneau, 1993; Dalton & Presnall, 1998). Such a mechanism is consistent with the characteristically high concentrations of incompatible elements, the high LREE/HREE ratios and the low Al contents in kimberlite (Mitchell, 1995).

Dalton & Presnall (1998) investigated melting of a model carbonated garnet lherzolite in the simple system CMAS–CO_2 at 6 GPa. Specifically, their experiments explored the phase equilibria attending small degrees of partial melting of an idealized carbonate-bearing peridotite (Table 6). These experiments document marked changes in melt composition over a very narrow range (0–1 vol. %) of melt fractions (F). The experiments produced carbonatite-like melts at near-solidus conditions (1380°C), whereas kimberlite melts were produced 70–100°C above the solidus. The work by Dalton & Presnall improves on that by Canil & Scarfe (1990) by providing tighter constraints on the compositions of the melts for low degrees of partial melting above the carbonated lherzolite solidus.

The experimental results of Dalton & Presnall (1998) are summarized in Table 6 and shown in Fig. 9. The compositions of the experimentally produced melts are shown as filled circles in CaO–MgO–SiO_2 (Fig. 9a and c) and CaO–MgO–CO_2 (Fig. 9b and d) projections. The arrow on the continuous line illustrates the change in melt composition (from carbonatite to kimberlite) as temperature rises and values of F increase. These experimental data do not provide an exact representation of natural systems. They involve isobaric melting and natural kimberlite magmas derive from a variety of depths. The experiments use a model mantle source that employs an arbitrary amount of carbonate and is, overall, a simpler composition than found in nature. Notwithstanding these limitations, the data provide a basis for interpreting our samples in terms of source region melting processes. The effects of pressure will be mainly to shift the position of the liquid curve. Also, kimberlite contains few other components of significance except for iron, which should not cause large changes in the phase relationships. H_2O, however, is an important component whose effects on this system are not well constrained.

The compositions of kimberlite samples from Jericho are compared with the experimentally produced melts in Fig. 9a and b. Bulk macrocrystal kimberlite plots well away from the trace of mantle melts; they lie towards the average composition of the macrocryst assemblage, which is dominated by olivine (e.g. label A in Fig. 9b). Conversely, compositions of aphanitic kimberlite (JD69 and JD82) lie closer to the trace of mantle melt compositions. Furthermore, compositions that lie slightly off the model liquid path are displaced in a direction consistent with small amounts of olivine fractionation (e.g. label F in Fig. 9b). Sample JD51, which has the lowest MgO content, shows the most extreme relative fractionation of olivine (Fig. 9a and b; filled square). The composition of sample LGS07 (Fig. 9a and b; crosses) plots off the model liquid line and is coincident with bulk kimberlite compositions. This is further corroboration that sample LGS07 is not representative of kimberlite melt but is a mixture of melt and milled macrocrysts.

*Table 6: Compositions of partial melts of carbonated lherzolite reported by Dalton & Presnall (1998) for small fractions (*F*) of melting*

	Experimental melt composition						Regression coefficient		
Sample:	KM14	KM57	KM55	KM56	KM45	KM53	*a*	*b*	*c*
F (%):	0·34	0·49	0·56	0·61	0·80	1·03			
SiO_2	5·79	20·37	24·38	27·24	32·45	36·23	−4·4365	−16·6988	56·9398
Al_2O_3	0·66	1·77	2·88	2·21	3·21	3·09	–1·4724	−1·7811	6·4105
MgO	20·91	26·00	27·43	27·69	28·42	29·57	−6·3014	−6·3095	41·9125
CaO	28·03	21·03	18·34	18·40	17·26	16·58	12·2298	9·8006	−5·2960
CO_2*	44·61	30·84	26·97	24·46	18·65	14·53	−0·0174	14·9917	0·02484

Melt compositions (wt %) are fitted to empirical equations of the form $w_i = aF + (b/F) + c$, where *i* indicates the individual oxide.
*Concentration is calculated by difference.

Compositions of other world-wide kimberlite bodies (Table 5) are plotted against the melt compositions of Dalton & Presnall (1990) in Fig. 9c and d. Included in these data are compositions from the Wesselton (Shee, 1986), Leslie (Berg & Carlson, 1998) and Dutoitspan (Berg, 1998) kimberlite bodies, as well as average compositions of kimberlite from South Africa and Siberia (Table 5). The Wesselton kimberlite plots close to the trace of model melts (Fig. 9c and d) and, as suggested by previous workers, is probably a good approximation of unfractionated primitive kimberlite melt (e.g. Eggler & Wendlandt, 1979; Edgar *et al.*, 1988; Foley, 1990). The compositions of the Leslie and Dutoitspan kimberlites lie off the model liquid path, within the field established by bulk kimberlites, and are controlled by macrocryst assemblages (Fig. 9c). The average kimberlite compositions (Table 5) span a wide range of compositions and plot on either side of the model mantle melt curve (Fig. 9c and d).

ORIGINS OF THE JERICHO KIMBERLITE

We have used the experimental work of Dalton & Presnall (1998) and our best estimates of unfractionated kimberlite magma from the Jericho kimberlite (JD69 and JD82) to constrain the mantle origins of this kimberlite. The geotherm for the Jericho peridotites and pyroxenites established by Kopylova *et al.* (1998*b*, 1999) and Russell & Kopylova (1999) suggests that the Jericho kimberlite originated at pressures of 6 GPa (>190 km) or greater, and at temperatures exceeding 1250°C. The experimental conditions employed by Dalton & Presnall (1998) included temperatures of 1380–1505°C and 6 GPa pressure; these represent conditions that are found close to the base of the petrological lithosphere for the Slave craton (Kopylova *et al.*, 1998) and parallel the minimum *P–T* formation conditions for the Jericho kimberlite.

Using the experimental data from Dalton & Presnall (1998) we have fitted the melt compositions to empirical expressions as a function of *F* (fraction of melt) of the form

$$w_i = a_i F + \frac{b_i}{F} + c_i \qquad (1)$$

where w_i is the weight percent of the *i*th oxide and a_i, b_i and c_i are the fit coefficients for each oxide. Table 6 lists the fitted coefficients determined by solving the overdetermined system of linear equations implied by the six experimental data points. The experimental data and the empirical curves relating melt composition to values of *F* are plotted in Fig. 10. Plotted as oxide wt % vs *F*, these empirical curves describe the data very well; however, they should not be projected beyond the bounds of the experimental data. Furthermore, the actual values of *F* strongly reflect the chosen starting composition (e.g. Dalton & Presnall, 1998).

These empirical expressions are used to analyse the primitive melt compositions from Jericho. The model can be used in two ways. First, it provides an objective measure of whether the natural composition is sufficiently close to the model curve of Dalton & Presnall (1998) to be considered a mantle melt. Second, for samples that pass the test, we will have estimates of the fraction of melt required to produce the kimberlite from the model source.

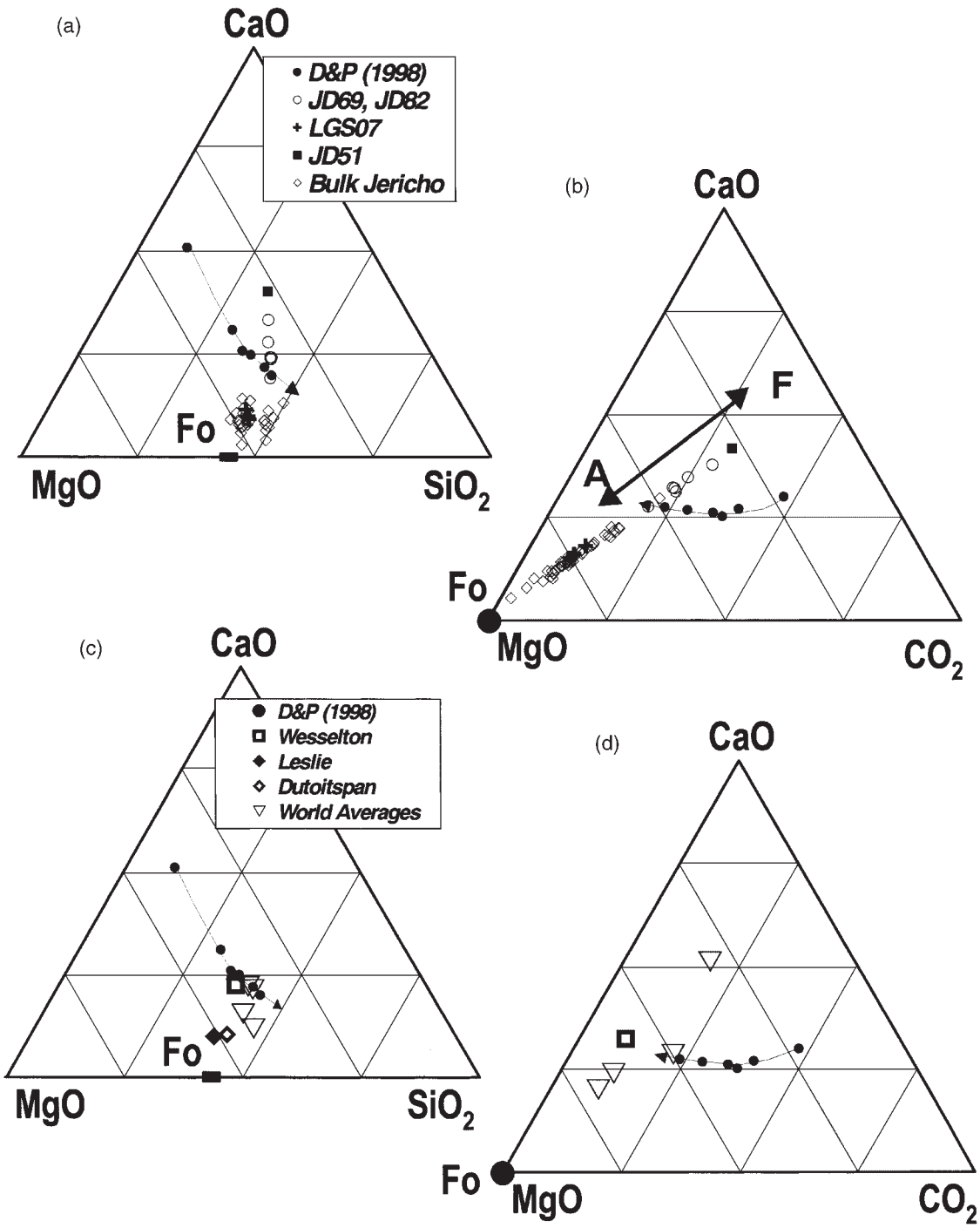

Fig. 9. Jericho kimberlite compositions (wt %) are plotted as CaO–MgO–SiO_2 (left) and CaO–MgO–CO_2 (right) and compared with experimental melt compositions of Dalton & Presnall (1998) (● and black arrow) produced by low ($\leq 1\%$) degrees of partial melting of carbonated garnet lherzolite: (a, b) comparison of aphanitic kimberlite with bulk kimberlite from Jericho; (c, d) Jericho primitive melt compositions compared with experimental melt compositions and with composition of other 'primitive' kimberlite magmas, including Wesselton (Shee, 1986), Leslie (Berg & Carlson, 1998), Dutoitspan (Berg, 1998) and other average kimberlite compositions (Ilupin & Lutz, 1971; Clement, 1982; Smith *et al.*, 1985) (see text and Table 5). Fo denotes compositional range of olivine from Fo_{88} to Fo_{100}. Labels A and F indicate the relative effects of accumulation of macrocrystic olivine and fractionation of olivine, respectively.

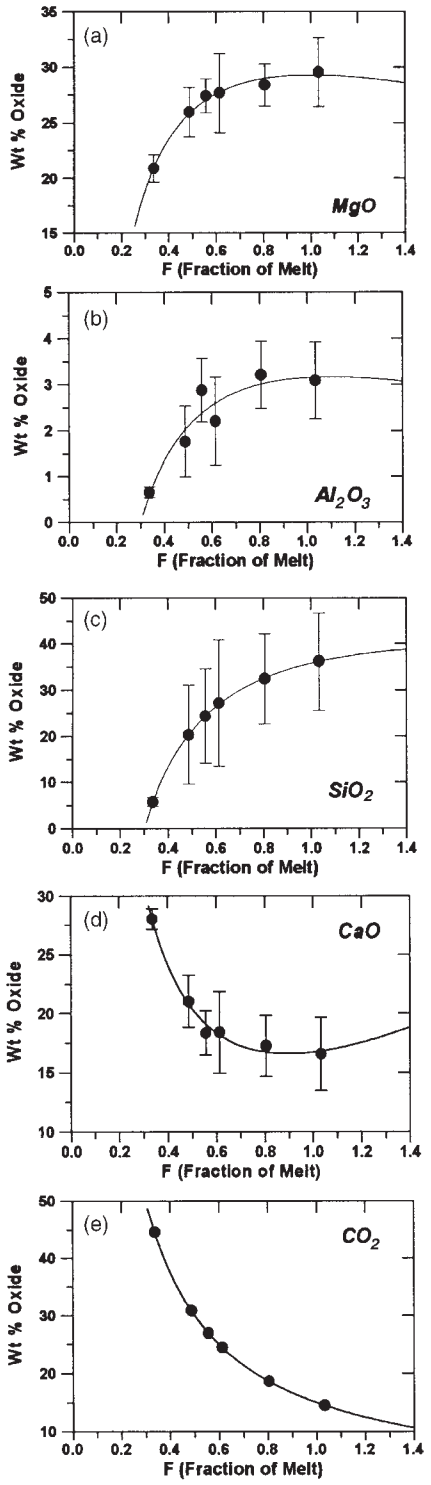

Fig. 10. Compositions of melts from experiments of Dalton & Presnall (1998) are plotted against F (fraction percent of melt) and compared with best-fit curves (Table 6) for each oxide: (a) MgO; (b) Al_2O_3; (c) SiO_2; (d) CaO; (e) CO_2. Vertical bars represent 1 SD analytical uncertainty reported by Dalton & Presnall (1998).

We solve for values of F for each kimberlite by minimization of the function

$$\text{sums of squares } (ssq) = \sum_{i}^{n}\left[\left(a_i F + \frac{b_i}{F} + c_i\right) - x_i\right]^2 \quad (2)$$

where a_i, b_i and c_i are the empirical fit coefficients for each of the n oxides (Table 6) and x_i is concentration of the ith oxide in the kimberlite. Minimization of this function provides for each rock an estimate of F and a measure of misfit (r.m.s.; Table 5).

Table 5 summarizes the results of these calculations applied to the samples of aphanitic chilled margins and to the Wesselton aphanitic kimberlite. These calculations indicate that samples JD69 and JD82 could be produced by 0·7–0·9% melting of the Dalton & Presnall (1998) idealized carbonated mantle source and that they fit the model melt curves well (Table 5). Samples JD51 and LGS07 cannot be fitted to the model as well; they have average residuals (r.m.s. values) that are 2–3 times larger than those for JD69 and JD82 (Table 5). The Wesselton kimberlite also appears to be a reasonable mantle melt and can be produced by 0·9% melting of the same source (Table 5).

Compositions of kimberlite from Jericho and Wesselton are plotted in terms of their measured values of MgO content and calculated model values of F in Fig. 11a and compared directly with the model curve for MgO (Table 6; Fig. 10a). Samples JD69 and JD82 and Wesselton are shown to fit the curve well. The same figure shows that samples of macrocrystal kimberlite and sample LGS07 cannot be derived by partial melting of this mantle source composition, at least under pressures of 6 GPa.

We elected to solve equation (2) by not including the mass balance relationship for CO_2 because of the difficulty of preserving the volatile species in natural systems (e.g. Foley, 1990; Girnis *et al.*,1995). Therefore, after obtaining a model value for F we were able to compute the apparent loss in CO_2 for each sample based on the rock's current CO_2 content:

$$CO_2^{Loss} = (a_{CO_2}F^* + \frac{b_{CO_2}}{F^*} + c_{CO_2}) - x_{CO_2} \quad (3)$$

where F^* is the model value of melt fraction for the specific kimberlite (Table 5). Figure 11b is a summary of model results for all of the aphanitic kimberlite samples from Jericho plotted as r.m.s. vs calculated CO_2 loss. Kimberlite compositions that can be exactly related to the mantle melt compositions of Dalton & Presnall (1998) should have near-zero values for r.m.s. and CO_2 loss. Conversely, those samples that cannot be reasonably related to the melting of the carbonate-bearing lherzolite will have r.m.s. values greater than analytical uncertainty and/or substantial values of lost CO_2. Samples JD69 and

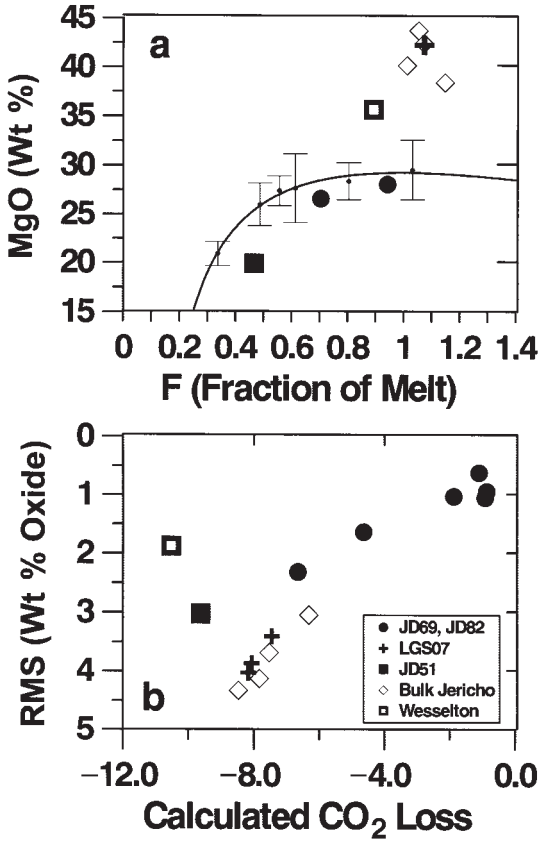

Fig. 11. Compositions of primitive kimberlite melts from Jericho and from Wesselton are interpreted in terms of percent melting of carbonated peridotite using model equations (Table 6) fitted to the experimental data of Dalton & Presnall (1998). Solutions are shown as (a) observed MgO content vs model melt fraction (F) and (b) degree of misfit (r.m.s.) vs the implied amount (wt %) of CO_2 lost. The best solutions feature low r.m.s. values and low calculated CO_2 loss (see text).

JD82 are described well by this model; they have low values of r.m.s. (<2) and the optimum solution requires little adjustment of CO_2 content (<2 wt %). These calculations suggest that the original kimberlite magma had CO_2 contents of 20 wt % and this is entirely consistent with high-pressure (e.g. >2 GPa) CO_2 solubility estimates for kimberlite melts (e.g. Brey *et al.*, 1991; Brey & Ryabchikov, 1994; Dreibus *et al.*, 1995). The Wesselton kimberlite also fits the model well (r.m.s. = 1·87) and must be considered a reasonable approximation to a primary melt. However, it is clear that, on the basis of the calculated CO_2 loss, the sample has lost substantial volatiles. In contrast, samples of LGS07 cannot be easily derived from this source by small fractions of melting; geochemically it has affinities to other macrocrystic phases of kimberlite from Jericho (Fig. 11b). JD51 is also inconsistent with being derived directly from partial melting of this mantle source (Table 5, Fig. 11b).

CONCLUDING DISCUSSION

Two aphanitic kimberlite samples (JD69 and JD82) collected from the Jericho kimberlite pipe, Canada, display textural and geochemical characteristics indicative of primitive kimberlite melts. Specifically, they display high *mg*-numbers (86–88) and have high concentrations of Ni (800–1400) and Cr (1300–1900). They also have elevated volatile contents, indicating minimal degassing during transport and emplacement, and rapid crystallization. The compositions of these primitive kimberlite melts are inferred to closely approximate primary kimberlite magma. We anticipate that these compositions will serve as improved starting compositions for experimental studies on kimberlite genesis (e.g. Eggler & Wendlandt, 1979; Edgar *et al.*, 1988; Arima *et al.*, 1993; Edgar & Charbonneau, 1993; Arima & Inoue, 1995; Girnis *et al.*, 1995; Wang & Gasparik, 2000).

The two kimberlite samples have measured CO_2 contents between 10 and 17 wt %, and these values provide important evidence on the minimum CO_2 contents of these exotic magmas. Our analysis indicates that the original CO_2 content may have been only 1–2 wt % higher than measured. Such high CO_2 contents are fully consistent with recent high-pressure volatile solubility studies on kimberlite (e.g. Brey *et al.*, 1991; Brey & Ryabchikov, 1994; Dreibus *et al.*, 1995; Girnis *et al.*, 1995) and most workers accept that kimberlite magmas can contain 20 wt % CO_2 in addition to significant H_2O. Experimental work also shows that these magmas must exsolve CO_2 during ascent, and that the exsolution is particularly intense during final emplacement (<3 km) and intensifies when the kimberlite magma breaks through to the surface.

The preservation of high CO_2 contents in our samples results from a combination of factors. First, all samples derive from the earliest phase of the Jericho kimberlite pipe, and most samples derive from relatively thin dykes. The implication is that these pulses of kimberlite had the greatest opportunity to quench and crystallize relatively quickly because of their small volume and the low ambient country rock temperatures. Second, all of these samples derive from the hypabyssal facies of the Jericho kimberlite (Phase 1). These rocks represent kimberlite that did not experience the intense fluidization that characterizes the upper diatreme facies. Third, although CO_2-rich fluids are being exsolved as deep as 100 km or more, they impart very high ascent velocities to the host magmas. For example, experimental studies of Canil & Fedortchouk (1999) suggest that the final rise and emplacement of kimberlite in the root zone of the Grizzly pipe took place in minutes. These very high ascent velocities operate to inhibit complete separation of the gas phase from the magma.

On the basis of these constraints, we suggest that samples JD69 and JD82 are the products of relatively

rapid crystallization of the original, highly gas-charged kimberlite magma dykes in the Jericho pipe. They perhaps represent kimberlite that was emplaced and quenched immediately before the final breakthrough of the pipe to the surface. The combination of high ascent rate, small volume magmas, thin dyke geometries and cool wall rocks led to the preservation of near-original magmatic gas contents.

Our data also bear on the debate concerning the depths of the source regions to Type I kimberlite (e.g. 200–300 km vs >400 km) although they cannot resolve the issue. A number of workers represented by the work of Ringwood *et al.* (1992) have argued that Group 1A kimberlite has a transition zone origin. Other workers (e.g. Eggler & Wendlandt, 1979; Bailey, 1980; Canil & Scarfe, 1990; Edgar & Charbonneau, 1993) have produced evidence that Group I kimberlite can be and is produced by partial melting of substantially shallower mantle (e.g. 5–8 GPa). We have shown that the compositions of samples JD69 and JD82 are consistent with small degrees of partial melting of carbonate-bearing garnet lherzolite at 6 GPa (Dalton & Presnall, 1998). Therefore, our data are at least permissive of derivation from melting a carbonated lherzolitic mantle at intermediate mantle pressures (e.g. above the transition zone). Such an origin would place the source region to the Jericho kimberlite at a depth equivalent to the uppermost asthenosphere beneath the north central Slave craton.

ACKNOWLEDGEMENTS

This research was funded entirely by the Industrially Oriented Research Partnership programme of NSERC through the generous support of Canamera Geological Ltd (1996–1998) and Lytton Minerals Ltd (1999). We are particularly appreciative of the support and encouragement of Dr Harrison Cookenboo. Our research benefited from open discussions with Greg Dipple, Kurt Kyser and Ian Coulson. Lastly, we are particularly indebted to Dante Canil, John Dalton and Bob Luth for their critical and thorough reviews; their comments and suggestions have led, in our opinion, to a much improved manuscript.

REFERENCES

Apter, D. B., Harper, F. J., Wyatt, B. A. & Smith, B. H. S. (1984). The geology of the Mayeng Kimberlite Sill Complex, South Africa. In: Kornprobst, J. (ed.) *Kimberlites. I: Kimberlites and Related Rocks. Vol. 11A, Developments in Petrology Series*. Amsterdam: Elsevier, pp. 43–57.

Arima, M. & Inoue, M. (1995). High pressure experimental study on growth and resorption of diamond in kimberlite melt. *Extended Abstracts, 6th International Kimberlite Conference*. Novosibirsk: United Institute of Geology, Geophysics and Mineralogy, Siberian Branch of the Russian Academy of Sciences Novosibirsk, pp. 8–10.

Arima, M., Nakayama, K., Akaishi, M., Yamaoka, S. & Kanda, H. (1993). Crystallization of diamond from a silicate melt of kimberlite composition in high-pressure and high-temperature experiments. *Geology* **21**, 968–970.

Bailey, D. K. (1980) Volatile flux, geotherms, and the generation of the kimberlite–carbonatite–alkaline magma spectrum. *Mineralogical Magazine* **43**, 695–699.

Berg, G. W. (1998). Geochemical relations which reflect the history of kimberlites from the type area of Kimberley, South Africa. *Extended Abstracts, 7th International Kimberlite Conference*. Cape Town: University of Cape Town, pp. 76–78.

Berg, G. W. & Carlson, J. A. (1998) The Leslie Kimberlite Pipe of Lac de Gras, Northwest Territories, Canada: evidence of near surface hypabyssal emplacement. *Extended Abstracts, 7th International Kimberlite Conference*. Cape Town: University of Cape Town, pp. 81–83.

Bhattacharji, S. (1967). Mechanics of flow differentiation in ultramafic and mafic sills. *Journal of Geology* **75**, 101–112.

Brey, G. P. & Ryabchikov, I. D. (1994). Carbon dioxide in strongly silica undersaturated melts and origin of kimberlite magmas. *Neues Jahrbuch für Mineralogie, Monatshefte* **10**, 449–463.

Brey, G. P., Kogarko, L. N. & Ryabchikov, I. D. (1991). Carbon dioxide in kimberlitic melts. *Neues Jahrbuch für Mineralogie, Monatshefte* **4**, 159–168.

Canil, D. & Fedortchouk, Y. (1999) Garnet dissolution and the emplacement of kimberlites. *Earth and Planetary Science Letters* **167**, 227–237.

Canil, D. & Scarfe, C. M. (1990). Phase relations in peridotite + CO_2 systems to 12 GPa: implications for the origin of kimberlite and carbonate stability in the Earth's upper mantle. *Journal of Geophysical Research* **95**, 15805–15816.

Clement, C. R. (1982). A comparative geological study of some major kimberlite pipes in the Northern Cape and Orange Free State. Ph.D. Thesis, University of Cape Town.

Cookenboo, H. O. (1998) Emplacement history of the Jericho kimberlite pipe, northern Canada. *Extended Abstracts, 7th International Kimberlite Conference*. Cape Town: University of Cape Town, pp. 161–163.

Dalton, J. A. & Presnall, D. C. (1998) The continuum of primary carbonatitic–kimberlitic melt compositions in equilibrium with lherzolite: data from the system $CaO–MgO–Al_2O_3–SiO_2–CO_2$ at 6 GPa. *Journal of Petrology* **39**, 1953–1964.

Dalton, J. A. & Wood, B. J. (1993) The compositions of primary carbonate melts and their evolution through wallrock reaction in the mantle. *Earth and Planetary Science Letters* **119**, 511–525.

Davis, W. J. (1991). Granitoid geochemistry and Late Archean crustal evolution in the central Slave province. Ph.D. Thesis, Memorial University of Newfoundland, St John's.

Deines, P. & Gold, D. P. (1973). The isotopic composition of carbonatite and kimberlite carbonates and their bearing on the isotopic composition of deep-seated carbon. *Geochimica et Cosmochimica Acta* **37**, 1709–1733.

Dreibus, G., Brey, G. & Girnis, A. (1995). The role of carbon dioxide in the generation and emplacement of kimberlite magmas: new experimental data on CO_2 solubility. *Extended Abstracts, 6th International Kimberlite Conference*. Novosibirsk: United Institute of Geology, Geophysics and Mineralogy, Siberian Branch of the Russian Academy of Sciences Novosibirsk, pp. 138–140.

Edgar, A. D. & Charbonneau, H. E. (1993). Melting experiments on a SiO_2-poor, CaO-rich aphanitic kimberlite from 5–10 GPa and their bearing on sources of kimberlite magmas. *American Mineralogist* **78**, 132–142.

Edgar, A. D., Arima, M., Baldwin, D. K., Bell, D. R., Shee, S. R., Skinner, M. W. & Walker, E. C. (1988). High-pressure–high-temperature melting experiments on a SiO_2-poor aphanitic

kimberlite from the Wesselton mine, Kimberley, South Africa. *American Mineralogist* **73**, 524–533.

Edwards, D., Rock, N. M. S., Taylor, W. R., Griffin, B. J. & Ramsay, R. R. (1992). Mineralogy and petrology of the Aries diamondiferous kimberlite pipe, Central Kimberley Block, Western Australia. *Journal of Petrology* **33**, 1157–1191.

Eggler, D. H. (1975) Peridotite–carbonate relations in the system $CaO–MgO–SiO_2–CO_2$. *Carnegie Institution of Washington Yearbook* **74**, 468–474.

Eggler, D. H. (1978) The effect of CO_2 upon partial melting of peridotite in the system $Na_2O–CaO–Al_2O_3–MgO–SiO_2–CO_2–H_2O$ to 35 kilobars, with an analysis of melting in a peridotite $H_2O–CO_2$ system. *American Journal of Science* **278**, 305–343.

Eggler, D. H. & Wendlandt, R. F. (1979). Experimental studies on the relationship between kimberlite magmas and partial melting of peridotite. In: Boyd, F. R. & Meyer, H. O. A. (eds) *Kimberlites, Diatremes and Diamonds: their Geology, Petrology and Geochemistry*. Washington, DC: American Geophysical Union, pp. 331–338.

Foley, S. F. (1990). A review and assessment of experiments on kimberlites, lamproites and lamprophyres as a guide to their origin. *Proceedings of the Indian Academy of Sciences (Earth and Planetary Sciences)* **99**, 57–80.

Girnis, A. V., Brey, G. P. & Ryabchikov, I. D. (1995). Origin of Group IA kimberlites: fluid-saturated melting experiments at 45–55 kbar. *Earth and Planetary Science Letters* **134**, 283–296.

Hoefs, J. (1997) *Stable Isotope Geochemistry*. Berlin: Springer.

Ilupin, I. P. & Lutz, B. G. (1971). The chemical composition of kimberlite and questions on the origin of kimberlite magmas. *Sovetskaya Geologiya* **6**, 61–73 (in Russian).

Jenner, G. A., Longerich, H. P., Jackson, S. E. & Fryer, B. J. (1990). ICP-MS: a powerful tool for high-precision trace-element analysis in earth sciences: evidence from analysis of selected U.S.G.S. reference samples. In: Potts, P. J., Dupuy, C. & Bowles, J. F. W. (eds) *Microanalytical Methods in Mineralogy and Geochemistry. Chemical Geology* **83**, 133–148.

Kirkley, M. B., Smith, H. B. & Gurney, J. J. (1989). Kimberlite carbonates—a carbon and oxygen stable isotope study. In: Ross, J. *et al.* (eds) *Kimberlites and Related Rocks. Geological Society of Australia Special Publication* **14**(1), 264–281.

Kobelski, B. J., Gold, D. P. & Deines, P. (1979). Variations in stable isotope compositions for carbon and oxygen in some South African and Lesothan kimberlites. In: Boyd, F. R. & Meyer, H. O. A. (eds) *Kimberlites, Diatremes and Diamonds: their Geology, Petrology and Geochemistry*. Washington, DC: American Geophysical Union, pp. 264–281.

Komar, P. D. (1972). Flow differentiation in igneous dykes and sills; profiles of velocity and phenocryst concentration. *Geological Society of America Bulletin* **83**, 3443–3447.

Kopylova, M. G., Russell, J. K. & Cookenboo, H. (1998*a*). Petrography and chemistry of the Jericho kimberlite (Slave Craton, Northern Canada). *Extended Abstracts, 7th International Kimberlite Conference*. Cape Town: University of Cape Town, pp. 449–451.

Kopylova, M. G., Russell, J. K. & Cookenboo, H. (1998*b*). Upper-mantle stratigraphy of the Slave craton, Canada: insights into a new kimberlite province. *Geology* **26**, 315–318.

Kopylova, M. G., Russell, J. K. & Cookenboo, H. (1999) Petrology of peridotite and pyroxenite xenoliths from the Jericho kimberlite: implications for the thermal state of the mantle beneath the Slave craton, northern Canada. *Journal of Petrology* **40**, 79–104.

Legault, M. I. & Charbonneau, B. W. (1993). Geophysical, geochemical, and petrographical study of the Contwoyto Batholith, Lupin gold mine area, Northwest Territories. In: *Current Research, Part E. Geological Survey of Canada, Paper* **93-1E**, 207–218.

McDonough, W. F., Sun, S., Ringwood, A. E., Jagoutz, E. & Hofmann, A. W. (1992). Potassium, rubidium, and cesium in the Earth and Moon and the evolution of the mantle of the Earth. *Geochimica et Cosmochimica Acta* **56**, 1001–1012.

Mitchell, R. H. (1986). *Kimberlites: Mineralogy, Geochemistry, and Petrology*. New York: Plenum.

Mitchell, R. H. (1995). *Kimberlites, Orangeites, and Related Rocks*. New York: Plenum.

Mitchell, R. H. (1997). *Kimberlites, Orangeites, Lamproites, Melilitites, and Minettes: a Petrological Atlas*. Thunder Bay, Ontario: Almaz Press, 243 pp.

Price, S. E. (1998) Primitive kimberlite magmas from Jericho, N.W.T., Canada: constraints on primary magma chemistry. M.Sc. Thesis, University of British Columbia, Vancouver.

Ringwood, A. E., Kesson, S. E., Hibberson, W. & Ware, N. (1992). Origin of kimberlites and related magmas. *Earth and Planetary Science Letters* **113**, 521–538.

Roeder, P. L. & Emslie, R. F. (1970) Olivine–liquid equilibrium. *Contributions to Mineralogy and Petrology* **29**, 275–289.

Russell, J. K. & Kopylova, M. G. (1999) A steady-state conductive geotherm for the North–central Slave, Canada: inversion of petrological data from the Jericho kimberlite pipe. *Journal of Geophysical Research* **104**, 7089–7101.

Russell, J. K. & Snyder, L. D. (1997) Petrology of picritic basalts from Kamloops, British Columbia: primary liquids from a Triassic–Jurassic arc. *Canadian Mineralogist* **35**, 521–541.

Scott Smith, B. H. (1996). Kimberlites. In: Mitchell, R. H. (ed.) *Undersaturated Alkaline Rocks: Mineralogy, Petrogenesis, and Economic Potential. Mineralogical Society of Canada, Short Course Series* **24**, 217–243.

Shee, S. R. (1986). The petrogenesis of the Wesselton mine kimberlites, Kimberley, South Africa. Ph.D. Thesis, University of Cape Town.

Sheppard, S. M. F. & Dawson, J. B. (1975). Hydrogen, carbon and oxygen isotope studies of megacryst and matrix minerals from Lesothan and South African kimberlites. *Physics and Chemistry of the Earth* **9**, 747–763.

Smith, C. B., Gurney, J. J., Skinner, E. M. W., Clement, C. R. & Ebrahim, N. (1985). Geochemical character of southern African kimberlites: a new approach based upon isotopic constraints. *Transactions of the Geological Society of South Africa* **88**, 267–280.

Sun, S. S. (1980). Lead isotopic study of young volcanic rocks from mid-ocean ridges, ocean islands and island arcs. In: Bailey, D. K., Tarney, J. & Dunham, K. (eds) *The Evidence for Chemical Heterogeneity in the Earth's Mantle. Philosophical Transactions of the Royal Society of London, Series A*, **297**, 409–445.

Taylor, S. R. & McLennan, S. M. (1985). *The Continental Crust: its Composition and Evolution*. Oxford: Blackwell.

Taylor, W. R., Tompkins, L. A. & Haggerty, S. E. (1994). Comparative geochemistry of West African kimberlites: evidence for a micaceous kimberlite end member of sublithospheric origin. *Geochimica et Cosmochimica Acta* **58**, 4017–4037.

Wang, W. & Gasparik, T. (2000). Melting of a primitive aphanitic kimberlite at 5–23 GPa. Implications for the origin of kimberlitic melts. *American Mineralogist* (submitted).

Wyllie, P. J. (1977) Mantle fluid compositions buffered in peridotite–CO_2–H_2O. *Journal of Geology* **85**, 187–208.

Wyllie, P. J. (1980) The origin of kimberlite. *Journal of Geophysical Research* **85**, 6902–6910.